



Trimming of silicon-on-insulator ring-resonators via localized laser annealing

VERA BIRYUKOVA,^{1,*} GRAHAM J. SHARP,¹ CHARALAMBOS KLITIS,¹  AND MARC SOREL^{1,2}

¹*School of Engineering, University of Glasgow, G12 8LT, United Kingdom*

²*Institute of Technologies for Communication, Information and Perception (TeCIP), Sant'Anna School of Advanced Studies, Via Moruzzi 1, 56127 Pisa, Italy*

**v.biryukova.1@research.gla.ac.uk*

Abstract: We propose a post-fabrication trimming method for the silicon-on-insulator photonic platform based on localised laser annealing of hydrogen silsesquioxane (HSQ) cladding. The technique is fast, does not degrade the device performance, does not require additional fabrication steps, and can therefore be implemented at minimal cost. Here we experimentally demonstrated how the spectrum of a ring resonator can be shifted by over 1 nm by annealing a section of the device as short as 30 μm , corresponding to a change in the effective refractive index of $\sim 10^{-2}$. Modifications of both the HSQ refractive index and its chemical structure as a function of the annealing temperature are also discussed. Trimming of multi-ring resonators indicate that this technique can be effectively used for post-fabrication reconfiguration of complex photonic circuits or to compensate for the fabrication tolerances of a typical CMOS process.

Published by The Optical Society under the terms of the [Creative Commons Attribution 4.0 License](https://creativecommons.org/licenses/by/4.0/). Further distribution of this work must maintain attribution to the author(s) and the published article's title, journal citation, and DOI.

1. Introduction

In recent years, silicon on insulator (SOI) has established itself as the dominant platform for integrated photonic circuits [1]. By and large its prominence is based on compatibility with the CMOS process and a compact device footprint enabled by the high index contrast between the silicon core and buried oxide (BOX) layers. A variety of active and passive devices have been successfully demonstrated showcasing potential applications of the platform in areas ranging from on-chip optical interconnect [2] to quantum information processing [3] and sensing [4]. However, the large refractive index contrast of SOI waveguides comes at a cost of extreme sensitivity to fabrication tolerance. Any fabrication process, no matter how advanced, introduces a degree of uncertainty in device dimension, whose impact on device performance scales with the refractive index contrast. This can be caused by several factors such as non-uniformity in the layer thicknesses of the SOI wafer or imperfections in the fabrication process itself. The problem is most apparent in interferometric devices such as ring resonators where sub-nanometre scale variations in waveguide dimensions can significantly shift the spectral response of the device. For example, in resonators implemented using typical single mode quasi-TE waveguides the amount of shift is proportional to the variation in waveguide dimensions, such that a change in width of 1 nm translates to approximately 1 nm shift in the spectral response [5]. This becomes particularly critical in designs that make use of cascaded resonators where a decrease in Q-factor can be observed due to a mismatch in resonant wavelength of individual devices. There are formally two approaches to remedy this: active tuning and post-fabrication trimming. Active tuning can be implemented by changing the refractive index of the core by either exploiting the thermos-optic coefficient using a thermal heater [6] or free-carrier dispersion using a pin junction [7]. While effective, this approach suffers from increased power consumption, which can be unacceptable in certain applications such as optical interconnects, where the target power

consumption is set in the order of pico-joules per bit [8]. Hence, the technique is best suited for use in cases where continuous reconfiguration of the circuit is required, as opposed to static correction for fabrication error.

Post-fabrication trimming on the other hand is a set and forget technique, which is typically achieved by permanently changing the refractive index of either the core or cladding material and hence does not require a constant supply of power. Examples of trimming via waveguide core modification include laser induced amorphisation and ablation [9], localised recrystallization of an ion implanted waveguide section via laser annealing [10] and trimming of hydrogenated amorphous silicon waveguide via UV irradiation [11]. Trimming of the waveguide cladding has been demonstrated via electron beam induced compaction and strain of SiO₂ [12], electron bleaching of chromophore-doped polymer [13], photodarkening of A₂S₃ glass by visible light exposure [14] and corrective etching of SiN films [15]. In [16] the authors have proposed the use of Hydrogen Silsesquioxane, a type of spin on glass, as a trimmable cladding and have carried out an initial investigation by curing HSQ clad devices in an oven.

In this work, we take this approach further and utilise a highly focused visible laser beam to anneal individual devices and hence provide the necessary locality to change the refractive index of a single device. HSQ is widely used in nano-fabrication of SOI integrated photonic circuits both as a high resolution e-beam resist as well as a cladding material due to its similarity to silica. Therefore, no additional fabrication steps are required in order to realise trimmable photonic chips. First, we investigate the annealing process by assessing the changes in the HSQ chemical structure and optical refractive index as a function of annealing temperature. Then, by using a laser beam, annealing of individual devices is demonstrated on single and coupled ring resonators. The same approach can be applied to a variety of standard photonic building blocks, such as directional couplers, Mach-Zehnder Interferometers, etc., and, most importantly, it can be used at wafer scale.

2. Structural properties of HSQ

HSQ was initially developed as a low-k dielectric for the electronics industry [17]. It has also gained popularity as a negative tone e-beam resist due to its high-resolution capabilities, resilience to etching and as a cladding material for photonic devices. The atomic structure of commercially available HSQ resin (a mixture of HSQ and methyl ketone (MIBK)) commonly referred to as Flowable Oxide (FOX) resembles clusters of partially formed cages that can be transformed into a silica like network by electron beam exposure or thermal processing. The effect of this transformation on the physical properties of HSQ films, such as refractive index and density, has been widely studied [18–23]. The properties of the cured film have been shown to depend not only on temperature and soak time, but also on a number of other parameters such as the thickness of the initial film and curing environment.

In order to obtain a benchmark for HSQ annealing via laser irradiation we first investigate the change in refractive index obtained by Rapid Thermal Annealing (RTA). Test sample processing was kept identical with the method subsequently used in the fabrication of HSQ cladding for SOI devices. An HSQ solution FOX 16 was spun at 3000 rpm on silicon samples, resulting in a film thickness of approximately 500 nm. The samples were then baked for 15 minutes on a 95 °C hotplate followed by a 24-hour bake in an oven at 180 °C. Following the bake, samples were annealed in an RTA in the temperature range 350 °C – 1150 °C for 1 minute with an individual sample allocated to each temperature. In order to mimic laser annealing the chamber was not evacuated such as to allow annealing in air.

The samples were characterised using a Wollam M-2000 ellipsometer and a Bruker VERTEX 70 FTIR spectrometer. Figure 1(a) shows the FTIR spectrum of the control sample (baked at 180 °C as previously described) as well as the samples annealed in the RTA at different temperatures. The peaks of interest in the FTIR spectrum are the Si-O-Si double peak around 1100 cm⁻¹, the

H-Si-O double peak centred around 850 cm^{-1} , the Si-H peak at 2250 cm^{-1} [23] and the broad Si-OH peak at 3350 cm^{-1} [24]. A close-up of the Si-O-Si and H-Si-O double peaks is shown in Fig. 1(b). The peaks at lower wavenumbers (830 cm^{-1} for H-Si-O and 1075 cm^{-1} for Si-O-Si) are typically associated with a network structure, while the peaks at higher wavenumbers (865 cm^{-1} for H-Si-O and 1128 cm^{-1} for Si-O-H) represent a cage-like structure [23]. The sample cured at $350\text{ }^{\circ}\text{C}$ exhibits a clear change in the ratio of the network to cage peak intensity. This is in good agreement with current literature and translates directly to a decrease in the refractive index [Fig. 1(c)] [18]. Further increase of temperature to $550\text{ }^{\circ}\text{C}$ causes an increase in the refractive index. This change can be attributed to the disassociation of the Si-H bond [20] as is seen in the FTIR spectrum. Formation of Si-OH bond can also be observed, which is typically associated with moisture uptake [24]. Curing at $750\text{ }^{\circ}\text{C}$ and $950\text{ }^{\circ}\text{C}$ yields little change in refractive index, however, there is still a clear change in the FTIR spectrum. The Si-O-Si peak intensity continues to increase while the Si-OH peak decreases at $750\text{ }^{\circ}\text{C}$ and then disappears at $950\text{ }^{\circ}\text{C}$, which would suggest that the two processes have an opposite effect on the refractive index. Finally, the maximum refractive index of 1.45, with a total refractive index increase of $\Delta n \sim 0.06$, is obtained for the sample cured at $1150\text{ }^{\circ}\text{C}$. Further increase in the Si-O-Si peak intensity between samples cured at $950\text{ }^{\circ}\text{C}$ and $1150\text{ }^{\circ}\text{C}$ suggests an oxidation of the film. The FTIR spectrum of HSQ sample cured at $1150\text{ }^{\circ}\text{C}$ closely resembles the spectra reported for TEOS films [25]. We note that the asymmetric nature of the Si-O-Si peak, with a broadening towards higher wavenumbers, is typical for SiO_2 films due to the presence of two vibrational modes [26] and is unrelated to the cage structure of HSQ.

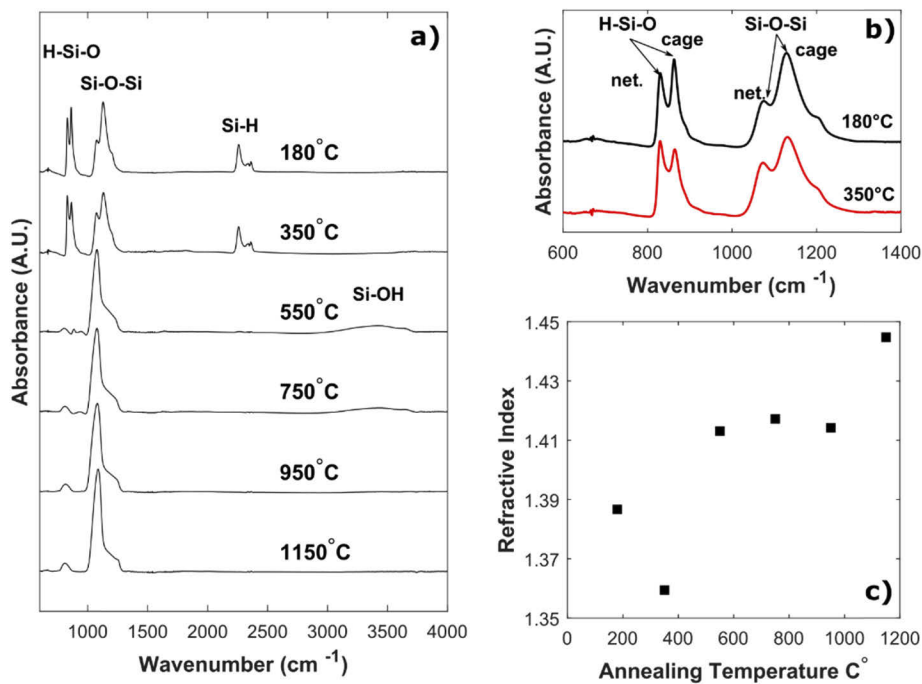


Fig. 1. (a) FTIR spectrum of HSQ films at different annealing temperatures; (b) An extract from the FTIR spectrum in the range $600\text{ to }1400\text{ cm}^{-1}$ showing the cage to network transition of HSQ; (c) refractive index of HSQ (at 1550 nm) as a function of curing temperature.

The following sections showcase how this change in refractive index can be applied for post-fabrication trimming of SOI devices.

3. Design and fabrication

The devices were realised using a standard waveguide geometry optimised for quasi-TE polarisation with a cross section of 500 nm in width and 220 nm in height, clad with a 500 nm thick HSQ layer [Fig. 2(a)]. The waveguides were defined by electron-beam lithography using ZEP520 resist and dry-etching with a $\text{SF}_6/\text{C}_4\text{F}_8$ chemistry. After the etch, the remaining mask was stripped using an oxygen ash and the layer of HSQ was spun on as a cladding. The sample was then baked on a hotplate at 95 °C for 15 minutes followed by a 24-hour bake at 180 °C in an oven as was done with the initial test samples. We note that these devices can also be fabricated using HSQ as an electron-beam resist. However, given that HSQ cannot be removed easily after silicon etching, the total attainable shift via laser annealing would be smaller due to the presence of electron beam cross-linked HSQ layer.

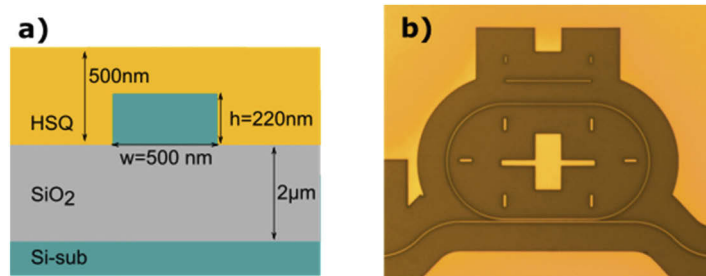


Fig. 2. a) Schematic view of HSQ clad silicon waveguide; b) Optical image of fabricated racetrack ring resonator.

Figure 2(b) shows an optical image of a race-track ring resonator fabricated using the process described above. The ring has a 30 μm coupling length and a 20 μm bend radius giving a Free Spectral Range (FSR) of approximately 3 nm. A set of alignment markers were placed around the ring to ensure accurate positioning of the laser beam during trimming, but far enough not to interfere with the optical properties of the device.

Trimming of the ring resonators was achieved by inducing a change in the refractive index of the cladding Δn_{HSQ} ; which in turn results in the change of the effective refractive index Δn_{eff} of the waveguide mode. Based on the results obtained via RTA processing we expect a maximum change in the refractive index of $\Delta n_{\text{HSQ}} \sim 0.06$; which corresponds to a change in the effective refractive index $\Delta n_{\text{eff}} = 9.55 \times 10^{-3}$. Furthermore, in an interferometric device such as a ring resonator, a change in the effective index translates to a change in spectrum given by $\Delta\lambda = \lambda_0 \Delta n_{\text{eff}} / n_g$. Thus, at a wavelength of 1550 nm we expect a maximum attainable shift of $\Delta\lambda = 3.63 \text{ nm}$ which is sufficient to compensate for parameter non-uniformity of a CMOS foundry process [27].

4. Trimming procedure and experimental results

Post-fabrication trimming was performed using the Witec Alpha 300 Micro-Raman tool, a simplified schematic of which is shown in Fig. 3(a). A green laser source (532 nm) was chosen for these experiments. During the exposure, the majority of the laser power is absorbed by the silicon waveguide generating heat, which in turn serves to anneal the overlying HSQ cladding.

Figure 3(b) shows a schematic view of the trimming process. The laser beam is focused on the sample using a $\times 20$ objective lens resulting in a $1/e^2$ beam radius of approximately 0.86 μm . This is followed by a semi-automated alignment process using a set of markers, developed especially for this experiment. Finally, the beam is scanned across the straight section of the device at a set speed using a piezoelectric stage.

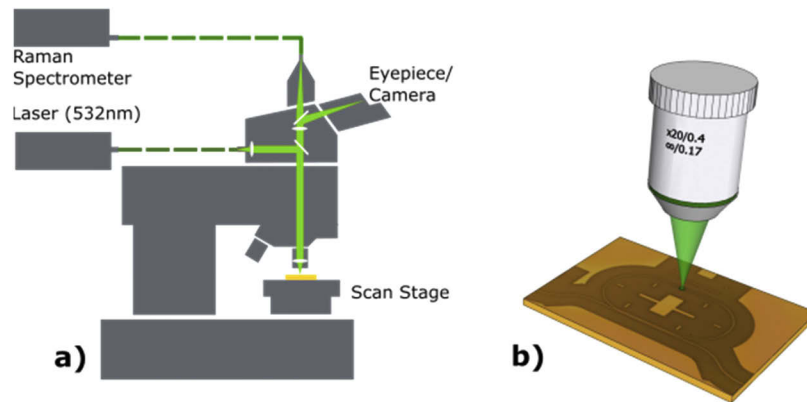


Fig. 3. a) Simplified schematic of the Witec alpha 300 tool used to perform the trimming, b) Schematic view of the trimming process.

For the first set of experiments, single racetrack ring resonators were annealed at a range of laser powers. The top section of the rings (30 μm) was exposed at a set speed of 1 $\mu\text{m/s}$. Figure 4(a) shows the permanent change in resonant wavelength as a function of laser power, with a maximum change of 1.1 nm. Furthermore, as can be seen from Fig. 4(b), there is no measurable change in the Q-factor before and after annealing ($Q \sim 16 \times 10^3$). This suggests that no additional losses were introduced by laser irradiation and that the coupling region remained unaffected.

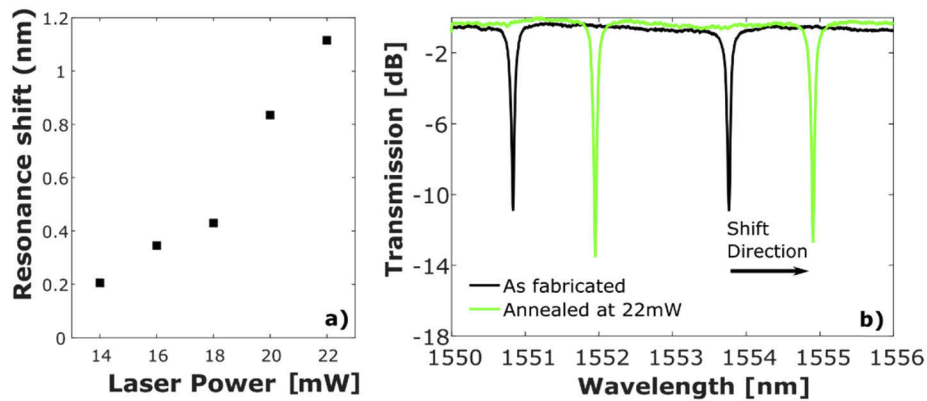


Fig. 4. (a) Shift in resonant wavelength as a function of laser power (b) Spectrum of a ring-resonator before and after trimming at 22 mW.

The temperature of the waveguide during annealing can be estimated based on the Raman spectrum. The position and width of the principle c-Si peak is temperature dependent and has been studied over a wide range temperatures [28]. Figure 5(a) shows the Raman spectrum of a silicon waveguide with a single peak at 520 cm^{-1} . This measurement was obtained at a low laser power of 4 mW, which does not cause any measurable change in the HSQ cladding. As the laser power is increased to 22 mW (the maximum power used in our experiments) two distinct peaks at 490 cm^{-1} and 520 cm^{-1} can be observed [Fig. 5(b)]. Similar behavior has been previously reported for silicon nano-crystals on silicon surface [29]. The peak at 520 cm^{-1} can be assigned to the wafer substrate that remains at low temperature, while the down shifted peak at 490 cm^{-1} indicates an increase of the waveguide temperature. We estimate that the temperature increase

of the waveguide caused by laser irradiation is approximately 1200 °C based on the value for Raman shift as a function of temperature provided in [28]. However, additional measurements based on the ratio of Stoke and anti-Stoke peak intensity may be desirable to further confirm this temperature estimate.

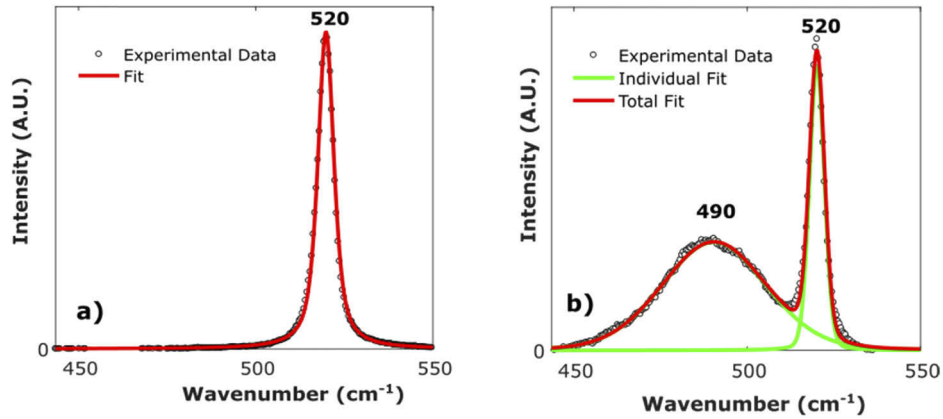


Fig. 5. (a) Raman spectrum of a silicon waveguide at low laser power (4 mW). (b) Raman spectrum of the same silicon waveguide during laser annealing at 22 mW, individual peaks have been fitted using a combination of Gaussian/Lorentzian functions.

For the second part of the experiment, the same technique was applied to two identical ring resonators coupled to the same waveguide. Figure 6(a) shows the spectrum of two nominally identical rings exhibiting distinct resonances due to fabrication tolerance. In order to correctly assign the resonant wavelengths and hence identify the ring that requires trimming, this measurement was coupled with infrared imaging of the scattered light from the ring resonators. The insert in Fig. 6(a) shows the scattered light gathered from the sample during this measurement. As can be observed, rings come into resonance at different times as the input wavelength is swept. In order to correct for this, trimming was performed at a fixed power of 22 mW. Note that the trimming range required in this case is smaller than that demonstrated in Fig. 4(a), therefore, annealing was performed by several consecutive single exposures until a good alignment of the two resonances has been obtained. As can be seen from Fig. 6(b), after trimming, the filter exhibits a single resonance with an improvement in the extinction ratio. Similarly, the insert shows the two rings scattering at the same time as the input wavelength is swept.

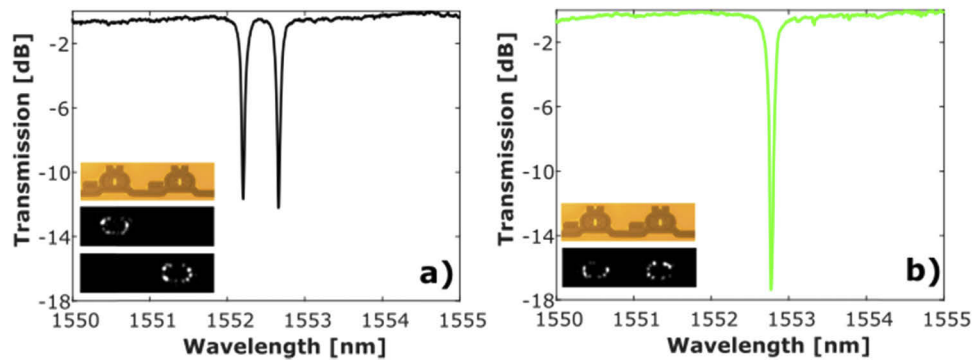


Fig. 6. a) Spectrum and infrared images showing scattered light from two nominally identical ring resonators before trimming, b) Spectrum and infrared images of the same two rings after trimming.

5. Discussion

We have experimentally demonstrated a resonance shift of up to 1.1 nm in a micro-ring resonator by localised laser annealing of a 30 μm -long waveguide section. In our experiments, the total annealing length was limited by stage movement and, as such, only a fraction of the device was exposed. Even so, this trimming range is sufficient to compensate for fabrication tolerance of a typical e-beam lithography process of ~ 0.5 nm [5]. The tolerance of a CMOS photolithography based process has been discussed in detail in [27]. The authors have demonstrated an inter-chip variation of 0.6 nm, which can be easily compensated for with the trimming range demonstrated here, and a chip-to-chip tolerance of 2 nm, which would require a larger section of the device to be exposed. Given that all trimming was performed at a speed of 1 $\mu\text{m}/\text{s}$, the chip-to-chip variation could still be adjusted for in under a minute of exposure. Furthermore, by paying a penalty in power and expanding the laser beam, as was done in [9], a trimming speed per device in the order of a few seconds could be obtained.

The measurements presented here have also demonstrated that there is no change in the Q-factor of the ring resonators after trimming. Firstly, this implies that the coupling region of the resonator remains unaltered during trimming and hence the proposed approach is highly localised. Given that the thermal conductivity of HSQ is very low and, based on previous work investigating tuning via metallic heaters [30], we expect that a separation of a few microns would be sufficient to achieve zero cross-talk between neighbouring devices during trimming. Secondly, the fact that the Q-factor remains unaltered suggests that laser irradiation and the subsequent modification in the HSQ bond structure has introduced no additional optical losses.

Finally, long term stability is of essence to any post-fabrication technique and has proven to be an issue for many of previously proposed approaches. One of the most common causes of parameter drift after trimming is moisture uptake. The FTIR data presented in Fig. 1(a) suggests that samples annealed in the temperature range of 550 $^{\circ}\text{C}$ – 750 $^{\circ}\text{C}$ will absorb water from the atmosphere, as is indicated by the presence of the Si-OH bond. However, we expect that samples annealed at lower or higher temperatures will be relatively stable. A further study of this is required and will be presented in future communication.

6. Conclusion

We have demonstrated how HSQ clad SOI devices can be permanently trimmed via localised laser annealing. This approach can be applied at wafer scale, at a low cost and does not require non-CMOS compatible materials or fabrication processes. Furthermore, the technique is

extremely fast and able to compensate for standard fabrication tolerance of a CMOS process in a matter of seconds.

As a proof of concept, an imperfect all-pass filter consisting of two racetrack ring resonators was trimmed to a single resonance. In addition, it has been shown that trimming did not induce a change in the Q-factor of the resonator implying that no additional loss was introduced to the waveguide and that the coupling region remained unaffected. This demonstrates that trimming is highly localised and can be used not only to tune the spectrum of individual devices, but also to selectively adjust specific areas of the same device.

All relevant data present in this publication can be accessed at [31].

Funding

Engineering and Physical Research Council (1804226, EP/L021129/1); H2020 Future and Emerging Technologies (829116).

Acknowledgments

The authors acknowledge the technical staff at the James Watt Nano-fabrication Centre at Glasgow University.

Disclosures

The authors declare no conflict of interest.

References

1. A. M. Urbas, Z. Jacob, L. Dal, D. Thomson, A. Zilkie, J. E. Bowers, and T. Komljenovic, "Roadmap on silicon photonics," *J. Opt.* **18**(7), 1–20 (2016).
2. A. H. Atabaki, S. Moazeni, F. Pavanello, H. Gevorgyan, J. Notaros, L. Alloatti, M. T. Wade, C. Sun, S. A. Kruger, H. Meng, K. Al Qubaisi, I. Wang, B. Zhang, M. A. Popović, V. M. Stojanović, R. J. Ram, A. Khilo, and V. Christopher, "for the Next Generation of Systems on a Chip," (2018).
3. J. Wang, J. Wang, S. Paesani, Y. Ding, R. Santagati, P. Skrzypczyk, A. Salavrakos, J. Tura, R. Augusiak, L. Man, D. Bacco, D. Bonneau, J. W. Silverstone, Q. Gong, A. Acín, K. Rottwitt, L. K. Oxenløwe, J. L. O. Brien, A. Laing, and M. G. Thompson, "Multidimensional quantum entanglement with large - scale integrated optics," *Science* **360**(6386), 285–291 (2018).
4. L. Detection, E. Luan, H. Shoman, D. M. Ratner, K. C. Cheung, and L. Chrostowski, "Silicon Photonic Biosensors Using Label-Free Detection," 1–42 (2018).
5. A. Samarelli, D. S. Macintyre, M. J. Strain, R. M. De La Rue, M. Sorel, and S. Thoms, "Optical characterization of a hydrogen silsesquioxane lithography process," *J. Vac. Sci. Technol., B: Microelectron. Nanometer Struct.–Process., Meas., Phenom.* **26**(6), 2290–2294 (2008).
6. J. E. Cunningham, I. Shubin, X. Zheng, T. Pinguet, A. Mekis, Y. Luo, H. Thacker, G. Li, J. Yao, K. Raj, and A. V. Krishnamoorthy, "Highly-efficient thermally-tuned resonant optical filters," *Opt. Express* **18**(18), 19055–19063 (2010).
7. Q. Xu, S. Manipatruni, B. Schmidt, J. Shakya, and M. Lipson, "12.5 Gbit/s carrier-injection-based silicon microring silicon modulators," *Opt. Express* **15**(2), 430–436 (2007).
8. D. A. B. Miller, "Optical interconnects to electronic chips," *Appl. Opt.* **49**(25), F59 (2010).
9. D. Bachman, Z. Chen, R. Fedosejevs, and Y. Y. Tsui, "Permanent fine tuning of silicon microring devices by femtosecond laser surface amorphization and ablation," *Opt. Express* **21**(9), 11048 (2013).
10. M. M. Milosevic, X. Chen, W. Cao, A. F. J. Runge, Y. Franz, C. G. Littlejohns, S. Mailis, A. C. Peacock, D. J. Thomson, and G. T. Reed, "Ion Implantation in Silicon for Trimming the Operating Wavelength of Ring Resonators," *IEEE J. Sel. Top. Quantum Electron.* **24**(4), 1–7 (2018).
11. T. Lipka, M. Kiepsch, and H. K. Trieu, "Hydrogenated amorphous silicon photonic device trimming by UV-irradiation," *Opt. Express* **22**(10), 12122–12132 (2014).
12. J. Schrauwen, D. Van Thourhout, and R. Baets, "Trimming of silicon ring resonator by electron beam induced compaction and strain," *Opt. Express* **16**(6), 3738 (2008).
13. S. Prorok, A. Y. Petrov, M. Eich, J. Luo, and A. K. Jen, "Trimming of high- Q -factor silicon ring resonators by electron beam bleaching," *Opt. Lett.* **37**(15), 3114–3116 (2012).
14. A. Canciamilla, F. Morichetti, S. Grillanda, P. Velha, M. Sorel, V. Singh, A. Agarwal, L. C. Kimerling, and A. Melloni, "Photo-induced trimming of chalcogenide-assisted silicon waveguides," *Opt. Express* **20**(14), 15807–17 (2012).

15. A. H. Atabaki, M. Askari, A. A. Eftekhar, and A. Adibi, "Accurate Post-Fabrication Trimming of Silicon Resonators," *9th Int. Conf. Gr. IV Photonics* 6, 42–44 (2012).
16. S. Spector, J. M. Knecht, and P. W. Juodawlkis, "Localized in situ cladding annealing for post-fabrication trimming of silicon photonic integrated circuits," *Opt. Express* **24**(6), 5996 (2016).
17. S. Jeng, K. Taylor, T. Seha, M. Chang, J. Fattaruso, and R. H. Havemann, "Highly Porous Interlayer Dielectric For Interconnect Capacitance Reduction," *1995 Symposium on VLSI Technology. Digest of Technical Papers*, 61–62 (1995).
18. C.-C. Yang and W.-C. Chen, "The structures and properties of hydrogen silsesquioxane (HSQ) films produced by thermal curing," *J. Mater. Chem.* **12**(4), 1138–1141 (2002).
19. C. W. Holzwarth, T. Barwicz, and H. I. Smith, "Optimization of hydrogen silsesquioxane for photonic applications," *J. Vac. Sci. Technol., B: Microelectron. Nanometer Struct.–Process., Meas., Phenom.* **25**(6), 2658 (2007).
20. Y. K. Siew, G. Sarkar, X. Hu, J. Hui, A. See, and C. T. Chua, "Thermal Curing of Hydrogen Silsesquioxane," *J. Electrochem. Soc.* **147**(1), 335 (2000).
21. S. Choi, M. J. Word, V. Kumar, and I. Adesida, "Comparative study of thermally cured and electron-beam-exposed hydrogen silsesquioxane resists," *J. Vac. Sci. Technol., B: Microelectron. Nanometer Struct.–Process., Meas., Phenom.* **26**(5), 1654 (2008).
22. H.-C. Liou and J. Pretzer, "Effect of curing temperature on the mechanical properties of hydrogen silsesquioxane thin films," *Thin Solid Films* **335**(1-2), 186–191 (1998).
23. M. Loboda, C. Grove, R. Schneider, and D. C. Corporation, "Properties of a-SiO_x: H Thin Films Deposited from Hydrogen Silsesquioxane Resins," *J. Electrochem. Soc.* **145**(8), 2861–2866 (1998).
24. A. A. Kumbhar, S. K. Singh, and R. O. Dusane, "Enhancement of moisture resistance of spin-on low-k HSQ films by hot wire generated atomic hydrogen treatment," *Thin Solid Films* **501**(1-2), 329–331 (2006).
25. J. P. Bange, L. S. Patil, and D. K. Gautam, "Growth and characterization of SiO₂ films deposited by flame hydrolysis deposition system for photonic device application," *Prog. Electromagn. Res. M* **3**, 165–175 (2008).
26. C. T. Kirk, "Quantitative analysis of the effect of disorder-induced mode coupling," *Phys. Rev. B* **38**(2), 1255–1273 (1988).
27. S. K. Selvaraja, W. Bogaerts, P. Dumon, D. Van Thourhout, and R. Baets, "Subnanometer Linewidth Uniformity in Silicon Nanophotonic Waveguide Devices Using CMOS Fabrication Technology," *IEEE J. Select. Topics Quantum Electron.* **16**(1), 316–324 (2010).
28. H. H. Burke and I. P. Herman, "Temperature dependence of Raman scattering in Ge_{1-x}Si_x alloys," *Phys. Rev. B* **48**(20), 15016–15024 (1993).
29. M. S. G. Mohammed, E. Cazzanelli, A. Fasanella, and M. Castriota, "Silicon Nanocrystals on the Surface of Standard Si Wafers: A Micro-Raman Investigation," *J. Mater. Sci. Chem. Eng.* **6**(7), 104–116 (2018).
30. D. Dai, L. Yang, and S. He, "Ultrasmall thermally tunable microring resonator with a submicrometer heater on Si nanowires," *J. Lightwave Technol.* **26**(6), 704–709 (2008).
31. "*", <https://dx.doi.org/10.5525/gla.researchdata.990>.